Response estimation for a floating bridge using acceleration output only

Petersen, Øyvind Wiig; Øiseth, Ole; Nord, Torodd Skjerve; Lourens, Eliz Mari

Publication date
2016

Document Version
Accepted author manuscript

Published in
Proceedings of ISMA 2016 - International Conference on Noise and Vibration Engineering

Citation (APA)
Petersen, Ø. W., Øiseth, O., Nord, T. S., & Lourens, E. M. (2016). Response estimation for a floating bridge using acceleration output only. In P. Sas, D. Moens, & A. van de Walle (Eds.), *Proceedings of ISMA 2016 - International Conference on Noise and Vibration Engineering : and USD2016 - International Conference on Uncertainty in Structural Dynamics* (pp. 613-625). KU Leuven.

Important note
To cite this publication, please use the final published version (if applicable).
Please check the document version above.

Paper published in: Proceedings of ISMA 2016 and USD2016, 19-21 Augustus 2017,
Leuven, Begium
ISBN: 978-94-6186-826-8
Editors: Sas P.,Moens D.,van de Walle A.

Response estimation for a floating bridge using acceleration output only

Øyvind Wiig Petersen [1], **Ole Øiseth** [1], **Torodd Skjerve Nord** [2], **Eliz-Mari Lourens** [3]
[1] NTNU, Norwegian University of Science and Technology, Department of Structural Engineering
7491 Trondheim, Norway
e-mail: **oyvind.w.petersen@ntnu.no**

[2] NTNU, Norwegian University of Science and Technology, Department of Civil and Transport Engineering
7491 Trondheim, Norway

[3] Delft University of Technology, Faculty of Civil Engineering and Geosciences
2628 CN Delft, The Netherlands

Abstract
The Norwegian Public Roads Administration is reviewing the possibility of using floating bridges as fjord crossings. The dynamic behaviour of very long floating bridges with novel designs are prone to uncertainties. Studying the dynamic behaviour of existing bridges is valuable for understanding the in-situ performance. We present a case study of the Bergsøysund Bridge, a 840 m long floating pontoon bridge located in Norway. An extensive monitoring system is installed on the bridge, including a network of accelerometers. A finite element model of the bridge is established. Using the measured acceleration output and recently developed Kalman filter based methods (a joint input-state (JIS) estimation algorithm and a dual Kalman filter (DKF)), we estimate accelerations at unmeasured locations. It is shown that the estimated response from the DKF agrees well with direct reference measurements. For the JIS, numerical instabilities in the estimates occur due to ill-conditioning of the matrices used in the system inversion.

1 Introduction

Understanding the dynamic response of civil engineering structures is important in order to build safe structures. In traditional design and dynamic analysis of structures, the response is obtained from an assumed load state together with an established model of the relevant structure. Uncertainties and errors in the structural model are thus propagated to the response. For unexplored or novel structural concepts, the degree of both model and loading uncertainty is higher compared to traditional ones. If the increased uncertainties are not met with any measures of improvement, the novel structures either face a higher probability of failure or can be overly costly since high uncertainties implies high partial factors in design.

A ferry-free E39 coastal highway project has been launched by the Norwegian Government. It aims to strengthen the highway and remove the need for ferries along the western coast of Norway, where most of the population lives. The area is dominated by fjords and surrounding mountains, making infrastructure such as tunnels and bridges indispensable. The fjords are typically 1-3 km wide and too deep for bottom-founded bridges. New solutions to fjord crossings are therefore being researched and reviewed, e.g. floating bridges, submerged tunnels and suspension bridges with floating towers. Common for all mentioned structures is that the dynamic behaviour is governed by fluid-structure interaction, which is typically more prone to uncertainties than of dynamics of dry structures.

By performing site monitoring of existing structures, it is possible to learn more about the true dynamic performance in complicated loading sceneries. In this contribution we present a case study of the Bergsøysund

Bridge, a floating pontoon bridge along the E39 coastal highway in mid-western Norway. With the help of recent developed techniques for system inversion, we estimate the dynamic response to ambient wave and wind loading using acceleration data measured at the bridge.

This paper applies two methods for estimating the dynamic response. The first is a joint-input state algorithm (JIS) for reduced order models [1], derived from minimum variance unbiased principles [2]. The method has been tested numerically [3–5] as well as experimentally [6–9]. Implementing the method in structural health monitoring schemes have also been proposed [10, 11], where the idea is to continuously monitor the remaining service life. The second method we apply is the recently published dual Kalman filter (DKF) [12–14], in which the states and forces are estimated from two filters working in conjunction.

2 Theory

2.1 Equations of motion for floating bridges

The governing equations of motion of a coupled fluid-structure system with n_{DOF} degrees of freedom (DOF) are for convenience first formulated in the the frequency domain:

$$-\omega^2\mathbf{M}(\omega)\mathbf{u}(\omega) + i\omega\mathbf{C}(\omega)\mathbf{u}(\omega) + \mathbf{K}(\omega)\mathbf{u}(\omega) = \mathbf{S}_{\text{ph}}\mathbf{p}_{\text{w}}(\omega) \tag{1}$$

where the displacement vector $\mathbf{u}(\omega)$ and the wave excitation forces $\mathbf{p}_{\text{w}}(\omega)$ are Fourier transforms of their time domain equivalents $\mathbf{u}(t) \in \mathbb{R}^{n_{DOF}}$ and $\mathbf{p}_{\text{w}}(t) \in \mathbb{R}^{n_p}$, respectively. The selection matrix $\mathbf{S}_{\text{ph}}$ assigns the wave forces to a designated set of DOF with direct fluid contact. Furthermore, the system matrices are split into two parts according to their nature of origin:

$$\mathbf{M}(\omega) = \mathbf{M}_{\text{s}} + \mathbf{M}_{\text{h}}(\omega) \tag{2}$$
$$\mathbf{C}(\omega) = \mathbf{C}_{\text{s}} + \mathbf{C}_{\text{h}}(\omega) \tag{3}$$
$$\mathbf{K} = \mathbf{K}_{\text{s}} + \mathbf{K}_{\text{h}} \tag{4}$$

$\mathbf{M}_s, \mathbf{C}_s$ and $\mathbf{K}_s$ are the mass, damping and stiffness matrices of the dry structure. The fluid-structure interaction gives rise to the hydrodynamic mass $\mathbf{M}_{\text{h}}(\omega)$ and damping $\mathbf{C}_{\text{h}}(\omega)$, both of which are functions of frequency. $\mathbf{K}_{\text{h}}$ is the hydrostatic restoring stiffness, which is assumed not to vary with frequency. By applying the inverse Fourier transform to Eq. 1 and rearranging, the equations of motion can also be formulated in the time domain as follows:

$$(\mathbf{M}_{\text{s}} + \mathbf{M}_{\text{h0}})\ddot{\mathbf{u}}(t) + \mathbf{C}_{\text{s}}\dot{\mathbf{u}}(t) + (\mathbf{K}_{\text{s}} + \mathbf{K}_{\text{h}})\mathbf{u}(t) = \mathbf{S}_{\text{ph}}\mathbf{p}_{\text{w}}(t) + \mathbf{S}_{\text{ph}}\mathbf{p}_{\text{mi}}(t) = \mathbf{S}_{\text{ph}}\mathbf{p}_{\text{h}}(t) \tag{5}$$

where $\mathbf{M}_{\text{h0}} = \mathbf{M}_h(\omega = 0)$. We define motion induced forces $\mathbf{p}_{\text{mi}}(t) \in \mathbb{R}^{n_p}$ by the following expression:

$$\mathbf{S}_{\text{ph}}\mathbf{p}_{\text{mi}}(t) = -\int_{-\infty}^{\infty} \dot{\mathbf{u}}(t-\tau)\tilde{\mathbf{k}}(\tau)\,\mathrm{d}\tau \tag{6}$$

The kernel $\tilde{\mathbf{k}}$ can be seen as an alternative rewriting of the retardation function often encountered in marine engineering [15]. Here, the definition of $\tilde{\mathbf{k}}$ follows from the Fourier convolution theorem:

$$\tilde{\mathbf{k}}(t) = \frac{1}{2\pi}\int_{-\infty}^{\infty} \left(i\omega(\mathbf{M}_{\text{h}}(\omega) - \mathbf{M}_{\text{h0}}) + \mathbf{C}_{\text{h}}(\omega)\right) e^{i\omega t}\,\mathrm{d}\omega \tag{7}$$

For the response estimation, a choice is made to establish a time-invariant linear system model. In what follows, the formulation in Eq. 5 is interpreted in the following way: the terms on the left hand side constitute a linear system, while the right hand side is the input forces applied to the linear system. The actual input forces are considered to be of less interest. For this reason, the motion induced and wave excitation forces are collected in the hydrodynamic force vector $\mathbf{p}_{\mathrm{h}}(t) = \mathbf{p}_{\mathrm{w}}(t) + \mathbf{p}_{\mathrm{mi}}(t)$. In other words, $\mathbf{p}_{\mathrm{h}}(t)$ is by definition the input forces as felt by the moving structure. $\mathbf{M}(\omega)$ and $\mathbf{C}(\omega)$ are not considered to be part of the linear system model; effects of the added mass and damping are considered as motion induced forces felt by a time-invariant system. As will be explained later, wind and traffic forces are neglected.

For large structures, it is often favoured to work with a set of $\mathrm{n_m}$ structural modes rather than a full model. Thus a reduced order model is constructed:

$$\mathbf{u}(t) = \mathbf{\Phi}\mathbf{z}(t) \tag{8}$$

where $\mathbf{z}(t) \in \mathbb{R}^{\mathrm{n_m}}$ is the modal coordinate vector and $\mathbf{\Phi} \in \mathbb{R}^{\mathrm{n_{DOF}} \times \mathrm{n_m}}$ contains the mass normalized mode shapes. When proportional damping of the linear system is assumed and Eq. 5 is premultiplied by $\mathbf{\Phi}^{\mathrm{T}}$ the modal equation reads:

$$\ddot{\mathbf{z}}(t) + \mathbf{\Gamma}\dot{\mathbf{z}}(t) + \mathbf{\Omega}^2\mathbf{z}(t) = \mathbf{\Phi}^{\mathrm{T}}\mathbf{S}_{\mathrm{ph}}\mathbf{p}_{\mathrm{h}}(t) \tag{9}$$

where $\mathbf{\Gamma} \in \mathbb{R}^{\mathrm{n_m} \times \mathrm{n_m}}$ and $\mathbf{\Omega} \in \mathbb{R}^{\mathrm{n_m} \times \mathrm{n_m}}$ are both diagonally populated with natural frequencies ω_j and modal damping ratios ξ_j:

$$\mathbf{\Omega} = \begin{bmatrix} \omega_1 & & & \\ & \omega_2 & & \\ & & \ddots & \\ & & & \omega_{\mathrm{n_m}} \end{bmatrix} \qquad \mathbf{\Gamma} = \begin{bmatrix} 2\omega_1\xi_1 & & & \\ & 2\omega_2\xi_2 & & \\ & & \ddots & \\ & & & 2\omega_{\mathrm{n_m}}\xi_{\mathrm{n_m}} \end{bmatrix} \tag{10}$$

The modal properties are found from the chosen linear model as discussed above, i.e. the system consisting of $\mathbf{M}_{\mathrm{s}}$, $\mathbf{C}_{\mathrm{s}}$, $\mathbf{K}_{\mathrm{s}}$ together with $\mathbf{K}_{\mathrm{h}}$ and $\mathbf{M}_{\mathrm{h0}}$. It is emphasized that the modal quantities do not correspond to solving a complex eigenvalue problem, which would include $\mathbf{M}_{\mathrm{h}}(\omega)$ and $\mathbf{C}_{\mathrm{h}}(\omega)$ (see [16] for details). Furthermore, a discrete time state-space representation of Eq. 9 is formulated under the assumption of a zero order hold on the force and a sample rate of $\frac{1}{\Delta t}$:

$$\mathbf{x}_{k+1} = \mathbf{A}\mathbf{x}_k + \mathbf{B}\mathbf{p}_{\mathrm{h},k} \tag{11}$$

$\mathbf{x}_k$ is the modal state vector and $\mathbf{p}_{\mathrm{h},k}$ is the force vector at time $t_k = k\Delta t$ $(k = 1 \ldots N)$:

$$\mathbf{x}_k = \begin{pmatrix} \mathbf{z}(t_k) \\ \dot{\mathbf{z}}(t_k) \end{pmatrix}, \quad \mathbf{p}_{\mathrm{h},k} = \mathbf{p}_{\mathrm{h}}(t_k) \tag{12}$$

The state transition matrix $\mathbf{A} \in \mathbb{R}^{2\mathrm{n_m} \times 2\mathrm{n_m}}$ and input matrix $\mathbf{B} \in \mathbb{R}^{2\mathrm{n_m} \times \mathrm{n_p}}$ are given as:

$$\mathbf{A} = e^{\mathbf{A}_{\mathrm{c}}\Delta t}, \quad \mathbf{B} = (\mathbf{A} - \mathbf{I})\mathbf{A}_{\mathrm{c}}^{-1}\mathbf{B}_{\mathrm{c}}, \quad \mathbf{A}_{\mathrm{c}} = \begin{bmatrix} \mathbf{0} & \mathbf{I} \\ -\mathbf{\Omega}^2 & -\mathbf{\Gamma} \end{bmatrix}, \quad \mathbf{B}_{\mathrm{c}} = \begin{bmatrix} \mathbf{0} \\ \mathbf{\Phi}^{\mathrm{T}}\mathbf{S}_{\mathrm{ph}} \end{bmatrix} \tag{13}$$

The application presented here is limited to acceleration output only. The output vector $\mathbf{y} \in \mathbb{R}^{\mathrm{n_{d,a}}}$ reads:

$$\mathbf{y}_k = \mathbf{S}_{\mathrm{a}}\ddot{\mathbf{u}}(t_k) = \mathbf{G}\mathbf{x}_k + \mathbf{J}\mathbf{p}_{\mathrm{h},k} \tag{14}$$

where $\mathbf{S}_\mathrm{a} \in \mathbb{R}^{\mathrm{n_{d,a}} \times \mathrm{n_{DOF}}}$ is a selection matrix describing the linear relationship between the output and the physical DOF. $\mathbf{G} \in \mathbb{R}^{\mathrm{n_{d,a}} \times \mathrm{n_m}}$ and $\mathbf{J} \in \mathbb{R}^{\mathrm{n_{d,a}} \times \mathrm{n_p}}$ symbolizes the output influence matrix and direct transmission matrix, respectively:

$$\mathbf{G} = -\mathbf{S}_\mathrm{a}\mathbf{\Phi}\begin{bmatrix}\mathbf{\Omega}^2 & \mathbf{\Gamma}\end{bmatrix}, \quad \mathbf{J} = \begin{bmatrix}\mathbf{S}_\mathrm{a}\mathbf{\Phi}\mathbf{\Phi}^\mathrm{T}\mathbf{S}_\mathrm{p}\end{bmatrix} \tag{15}$$

In the presence of noise, zero mean white noise vectors are added to Eq. 11 and 14, which completes the stochastic state-space representation:

$$\mathbf{x}_{k+1} = \mathbf{A}\mathbf{x}_k + \mathbf{B}\mathbf{p}_{\mathrm{h},k} + \mathbf{w}_k \tag{16}$$

$$\mathbf{y}_k = \mathbf{G}\mathbf{x}_k + \mathbf{J}\mathbf{p}_{\mathrm{h},k} + \mathbf{v}_k \tag{17}$$

The process noise $\mathbf{w}_k$ and measurement noise $\mathbf{v}_k$ are assumed to have the following covariance relations:

$$\mathbb{E}[\mathbf{w}_k\mathbf{w}_l^\mathrm{T}] = \mathbf{Q}\,\delta_{kl} \quad , \quad \mathbb{E}[\mathbf{v}_k\mathbf{v}_l^\mathrm{T}] = \mathbf{R}\,\delta_{kl} \quad , \quad \mathbb{E}[\mathbf{w}_k\mathbf{v}_l^\mathrm{T}] = \mathbf{0} \tag{18}$$

Additionally, a Guassian random walk is assumed for the DKF force evolution:

$$\mathbf{p}_{\mathrm{h},k+1} = \mathbf{p}_{\mathrm{h},k} + \boldsymbol{\eta}_k \tag{19}$$

$\boldsymbol{\eta}_k$ is also a zero mean white noise vector, with covariance $\mathbb{E}[\boldsymbol{\eta}_k\boldsymbol{\eta}_k^\mathrm{T}] = \mathbf{Q}_p$.

2.2 Response estimation methodology

Two methods will be used to estimate the response from a limited set of acceleration data, namely a JIS estimation algorithm [1] and the recently developed DKF [12]. Both are based on the widely popular Kalman Filter [17]. The equations for the two algorithms are given below. We recommend looking into the original works for the more details about the assumptions behind the filters. In addition, we especially point out the necessity of matrix reduction in the JIS for the removal of numerical instabilities when the number of measurements exceeds the model order ($\mathrm{n_d} > \mathrm{n_m}$), as is often the case for large bridges. Details can be found in [1].

Joint input-state estimation:

Initial quantities:

$$\text{State estimate:} \quad \hat{\mathbf{x}}_{0|-1} \tag{20}$$

$$\text{State error covariance:} \quad \mathbf{P}_{0|-1} \tag{21}$$

Input estimation:

$$\tilde{\mathbf{R}}_k = \mathbf{G}\mathbf{P}_{k|k-1}\mathbf{G}^\mathrm{T} + \mathbf{R} \tag{22}$$

$$\mathbf{M}_k = (\mathbf{J}^\mathrm{T}\tilde{\mathbf{R}}_k^{-1}\mathbf{J})^{-1}\mathbf{J}^\mathrm{T}\tilde{\mathbf{R}}_k^{-1} \tag{23}$$

$$\hat{\mathbf{p}}_{k|k} = \mathbf{M}_k(\mathbf{y}_k - \mathbf{G}\hat{\mathbf{x}}_{k|k-1}) \tag{24}$$

$$\mathbf{P}_{\mathbf{p}[k|k]} = (\mathbf{J}^\mathrm{T}\tilde{\mathbf{R}}_k^{-1}\mathbf{J})^{-1} \tag{25}$$

Measurement update:

$$\mathbf{L}_k = \mathbf{P}_{k|k-1}\mathbf{G}^{\mathrm{T}}\tilde{\mathbf{R}}_k^{-1} \tag{26}$$

$$\hat{\mathbf{x}}_{k|k} = \hat{\mathbf{x}}_{k|k-1} + \mathbf{L}_k(\mathbf{y}_k - \mathbf{G}\hat{\mathbf{x}}_{k|k-1} - \mathbf{J}\hat{\mathbf{p}}_{k|k}) \tag{27}$$

$$\mathbf{P}_{k|k} = \mathbf{P}_{k|k-1} - \mathbf{L}_k(\tilde{\mathbf{R}}_k - \mathbf{J}\mathbf{P}_{\mathbf{p}[k|k]}\mathbf{J}^{\mathrm{T}})\mathbf{L}_k^T \tag{28}$$

$$\mathbf{P}_{\mathbf{xp}[k|k]} = \mathbf{P}_{\mathbf{px}[k|k]}^{\mathrm{T}} = -\mathbf{L}_k\mathbf{J}\mathbf{P}_{\mathbf{p}[k|k]} \tag{29}$$

Time update:

$$\hat{\mathbf{x}}_{k+1|k} = \mathbf{A}\hat{\mathbf{x}}_{k|k} + \mathbf{B}\hat{\mathbf{p}}_{k|k} \tag{30}$$

$$\mathbf{P}_{k+1|k} = \begin{bmatrix}\mathbf{A} & \mathbf{B}\end{bmatrix}\begin{bmatrix}\mathbf{P}_{k|k} & \mathbf{P}_{\mathbf{xp}[k|k]} \\ \mathbf{P}_{\mathbf{px}[k|k]} & \mathbf{P}_{\mathbf{p}[k|k]}\end{bmatrix}\begin{bmatrix}\mathbf{A}^{\mathrm{T}} \\ \mathbf{B}^{\mathrm{T}}\end{bmatrix} + \mathbf{Q} \tag{31}$$

Dual Kalman Filter:

Initial quantities:

$$\text{Force estimate:} \quad \hat{\mathbf{p}}_0 \tag{32}$$

$$\text{Force error covariance:} \quad \mathbf{P}_0^{\mathrm{p}} \tag{33}$$

$$\text{State estimate:} \quad \hat{\mathbf{x}}_0 \tag{34}$$

$$\text{State error covariance:} \quad \mathbf{P}_0 \tag{35}$$

Prediction of the input:

$$\mathbf{p}_k^- = \mathbf{p}_{k-1} \tag{36}$$

$$\mathbf{P}_k^{p-} = \mathbf{P}_{k-1}^p + \mathbf{Q}_p \tag{37}$$

$$\tag{38}$$

Kalman gain and filter estimate for the input:

$$\mathbf{G}_k^p = \mathbf{P}_k^{p-}\mathbf{J}^T(\mathbf{J}\mathbf{P}_k^{p-}\mathbf{J}^T + \mathbf{R})^{-1} \tag{39}$$

$$\hat{\mathbf{p}}_k = \mathbf{p}_k^- + \mathbf{G}_k^p(\mathbf{d}_k - \mathbf{G}\hat{\mathbf{x}}_{k-1} - \mathbf{J}\mathbf{p}_k^-) \tag{40}$$

$$\mathbf{P}_k^p = \mathbf{P}_k^{p-} - \mathbf{G}_k^p\mathbf{J}\mathbf{P}_k^{p-} \tag{41}$$

Prediction of the state:

$$\mathbf{x}_k^- = \mathbf{A}\hat{\mathbf{x}}_{k-1} + \mathbf{B}\hat{\mathbf{p}}_k \tag{42}$$

$$\mathbf{P}_k^- = \mathbf{A}\mathbf{P}_{k-1}\mathbf{A}^T + \mathbf{Q} \tag{43}$$

Kalman gain and filter estimate for the state:

$$\mathbf{G}_k^x = \mathbf{P}_k^-\mathbf{G}^T(\mathbf{G}\mathbf{P}_k^-\mathbf{G}^T + \mathbf{R})^{-1} \tag{44}$$

$$\hat{\mathbf{x}}_k = \mathbf{x}_k^- + \mathbf{G}_k^x(\mathbf{d}_k - \mathbf{G}\mathbf{x}_k^- - \mathbf{J}\hat{\mathbf{p}}_k) \tag{45}$$

$$\mathbf{P}_k = \mathbf{P}_k^- - \mathbf{G}_k^x\mathbf{G}\mathbf{P}_k^- \tag{46}$$

Figure 1: The Bergsøysund Bridge. Photograph: K.A. Kvåle.

2.3 Conditions for response estimation

In the following, necessary conditions for successful response estimation is briefly discussed. Maes et al. [18] presented the fundamental requirements for instantaneous system inversion when modally reduced order models are used. Whether or not the requirements are met depends on the model representation as well as the sensor network. Good results are however not guaranteed even if the requirements are met; they only reflect the estimation feasibility from an algorithmic point of view. The requirements relevant for response estimation at the Bergsøysund Bridge is mentioned below.

Firstly, system observability is necessary for state estimation. In the case of acceleration output only, observability is fulfilled if and only if the matrix $\mathbf{S}_\mathrm{a}\mathbf{\Phi}$ has no zero columns. This means all the modes in the model must have an influence on the acceleration output.

Secondly, in order for the system to be instantaneously invertible, the rank of the matrix $\mathbf{J}$ in Eq. 14 must be equal to $\mathrm{n_p}$. This implies that the number of accelerations in the output, $\mathrm{n_{d,a}}$, must be greater or equal to the number of unknown forces, $\mathrm{n_p}$. In addition, $\mathrm{n_p}$ must not exceed the number of modes in the model ($\mathrm{n_m} \geq \mathrm{n_p}$).

Lastly, the presence of transmission zeros determines the stability of the solution. A transmission zero $\lambda_j \in \mathbb{C}$ is defined by the following equation:

$$\begin{bmatrix} \mathbf{A} - \lambda_j \mathbf{I} & \mathbf{B} \\ \mathbf{G} & \mathbf{J} \end{bmatrix} \begin{bmatrix} \mathbf{x}_0 \\ \mathbf{p}_{\mathrm{h},0} \end{bmatrix} = \begin{bmatrix} \mathbf{0} \\ \mathbf{0} \end{bmatrix} \tag{47}$$

When transmission zeros are present, the force $\mathbf{p}_{\mathrm{h},k} = \mathbf{p}_{\mathrm{h},0}\lambda_j^k$ $(k = 0, 1, \ldots N)$ will not be distinguishable from the output, thereby making a unique system inversion impossible. It can be shown that a so-called marginally stable transmission zero ($\lambda_j = 1$) always occurs when only acceleration outputs are available. Owing to the fact that static forces always remain undistinguishable by accelerometers, measurements of displacement or strains need be included in the output to eliminate the transmission zeros. In practical terms, a slow frequency drift in the state and force estimates are observed under marginally stability. Is it usually possible to filter out the drift.

3 Case study: the Bergsøysund Bridge

3.1 Description of the bridge and sensor network

Located in mid-western Norway, the Bergsøysund Bridge (see Fig. 1) is part of the E39 highway running along the west coast. The water depth in the strait reaches 300 m, making a bottom-founded bridge an impractical solution. A floating pontoon bridge was therefore chosen when it was built in 1992. The bridge has a 840 m long floating span with free spans of 105 m between the pontoons. In total, seven concrete

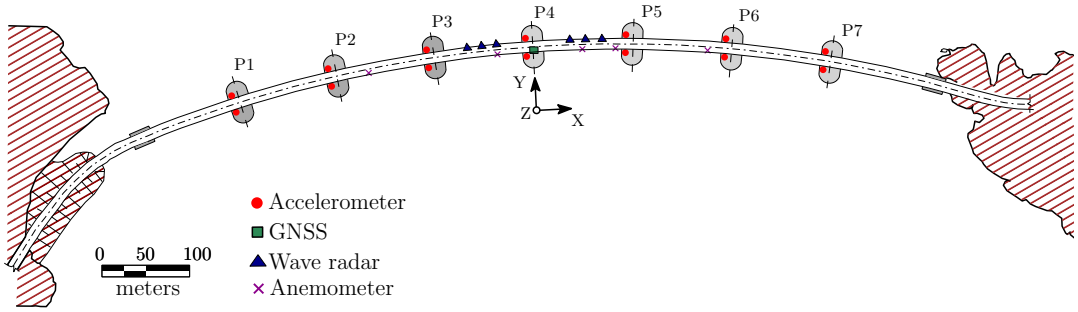

Figure 2: Monitoring system at the Bergsøysund Bridge

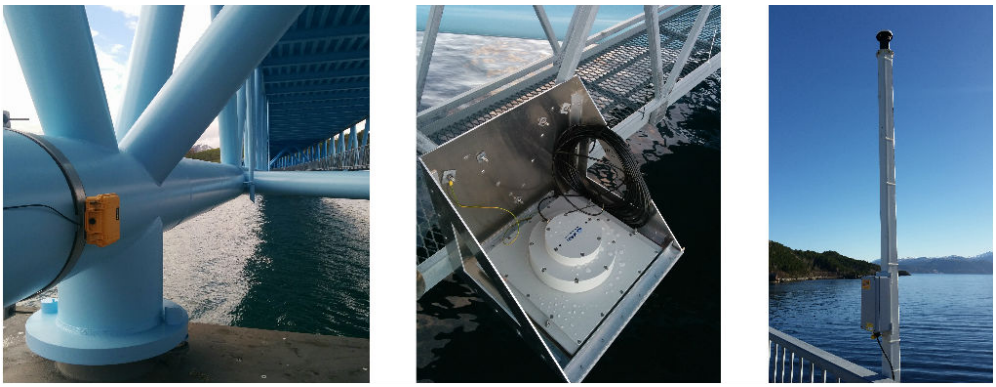

Figure 3: Selected instruments in the monitoring system. Left: accelerometer; middle: wave elevation radar; right: GNSS station. Photograph: K.A. Kvåle.

pontoons support the steel truss superstructure. At the ends, neoprene bearings and axial steel rods anchors the bridge to bedrock. The bridge is susceptible to dynamic excitations from wave actions, making it an interesting case study.

An extensive monitoring system is installed at the bridge as part of the E39 coastal highway research project. The sensor network consists of accelerometers, wave elevation radars, anemometers and a GNSS (Global Navigation Satellite System) station, shown Fig. 2 and 3. When predefined trigger values in wind velocity are exceeded, data is automatically recorded and saved. Data can either be retrieved locally or sent over the mobile internet network. The data most relevant for response estimation is the accelerometer output. Two triaxial accelerometers are installed at each pontoon. A more comprehensive description of the monitoring system is given in [19].

3.2 System model

The structural mass and stiffness matrices are obtained from a finite element (FE) model of the dry structure. Shown in Fig. 4, a model is created in the FE software ABAQUS using 3-node Timoshenko beam elements for the truss and shell elements for the stiffened upper deck. The hydrostatic stiffness matrix $\mathbf{K}_\mathrm{h}$ is obtained in the software DNV HydroD WADAM. The pontoons, assumed to behave as rigid bodies, are discretized as a single node with 6 DOF, to which the pontoon inertia as well as the hydrodynamic properties are assigned. A Rayleigh model is assumed for the structural damping of the linear system in Eq. 5:

$$\mathbf{C}_\mathrm{s} = \alpha(\mathbf{M}_\mathrm{s} + \mathbf{M}_\mathrm{h0}) + \beta(\mathbf{K}_\mathrm{s} + \mathbf{K}_\mathrm{h}) \tag{48}$$

The dry structure is assumed to be lightly damped, the values $\alpha = 5 \times 10^{-3}$ and $\beta = 10^{-3}$ are assigned.

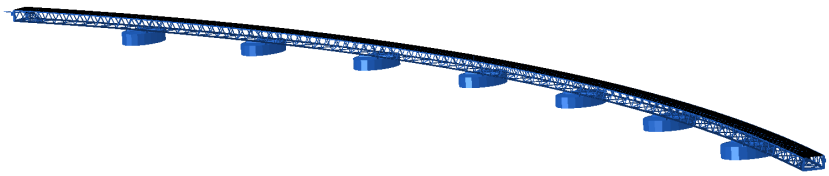

Figure 4: Finite element model of the Bergsøysund Bridge

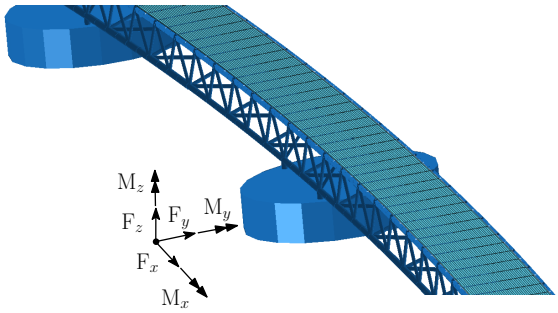

Figure 5: Definition of the force and moment directions on the pontoons

We remark that the hydrodynamic matrices $\mathbf{M}_\mathrm{h}(\omega)$ and $\mathbf{C}_\mathrm{h}(\omega)$ can also be acquired from DNV HydroD WADAM. However, in accordance with Eq. 5, we repeat that the frequency dependent matrices are not considered part of the linear system model, but rather as input forces. It is possible to construct a state-space model which includes the hydrodynamic mass and damping [15], but this option is beyond the scope of this paper.

While input estimation is not the primary goal in this contribution, the location of the external forces must be defined. The hydrodynamic forces are not considered as spatially distributed but rather as six force resultants working in the gravity centre of each pontoon. Thus $6 \times 7 = 42$ modelled wave forces are acting on the pontoons. A choice is made to neglect the force components Fx, My and Mz as defined in Fig. 5. As shown in numerical simulations of the bridge [20], the influence on the output from the discarded forces is negligible. They are also significantly smaller than the remaining components Fy, Fz and Mx when the mean wave direction is approximately perpendicular to the bridge. Thus the number of unknown forces is set to $\mathrm{n_p} = 3 \times 7 = 21$. Other sources of ambient excitation are assumed to be negligible or filtered out as noise. The response to traffic loading is largely removed by a lowpass filter and the wind forces are by nature significantly smaller compared to the hydrodynamic forces.

Next, a choice of modes for the reduced order model should be made. It is desired to exclude modes having very little influence on the output or modes which the forces cannot control [11]. If the modes are not removed, the system can suffer from ill-conditioning, giving rise to inaccurate estimates when noise is present. There is no significant contribution in the output data above 2 Hz. Consequently the 29 lowermost modes are considered, of which the lowest and highest natural frequency are 0.103 Hz and 1.93 Hz. Since the location of the sensors and forces is predetermined, we seek to eliminate modes which has poor influence on the output or which is not excited by the forces. This can be done by mapping the modal projection matrices $\mathbf{S}_\mathrm{a}\mathbf{\Phi}$ and $\mathbf{\Phi}^\mathrm{T}\mathbf{S}_\mathrm{p}$. Details are omitted here, see e.g. [18] for a tutorial. Two modes are removed, a total of $\mathrm{n_m} = 27$ modes are included in the model. It is however hard to give any further physical interpretation of these modes given the choice of the linear model, seeing that the modes do not directly represent the system in Eq. 1.

4 Estimation of dynamic response

A data time series recorded on November 8th 2015 is considered. Approximated from 10 minute intervals, the significant wave height ranged between 0.5–0.7 m and the mean wind velocity varied between 9 m/s and 16 m/s. The recorded acceleration data is originally sampled at 200 Hz, but is lowpass filtered (Chebyshev Type II at 5 Hz) and resampled to 10 Hz for the presented application.

In the demonstration of response estimation, one of the accelerometers at pontoon 3 (cf. Fig. 2) is left out to serve as a reference sensor. The remaining $\mathrm{n_{d,a}} = 39$ accelerometer signals constitute the sensor network. The acceleration at an unmeasured location is estimated analogous to Eq. 14:

$$\hat{\mathbf{y}}_k = \mathbf{G}'\hat{\mathbf{x}}_k + \mathbf{J}'\hat{\mathbf{p}}_{\mathrm{h},k} \tag{49}$$

where $\hat{\mathbf{x}}_k$ and $\hat{\mathbf{p}}_{\mathrm{h},k}$ are the state and force estimates obtained from the filters and $\mathbf{G}'$ and $\mathbf{J}'$ are constructed from Eq. 15 according to the new designated location. The following diagonal covariance matrices are used:

$$\mathbf{Q} = \mathrm{diag}(\ [\mathbf{10}]_{1\times 19} \quad [\mathbf{1}]_{1\times 8} \quad [\mathbf{10}]_{1\times 19} \quad [\mathbf{1}]_{1\times 8}\ ) \tag{50}$$

$$\mathbf{R} = 5 \times 10^{-2} \times \mathbf{I} \tag{51}$$

$$\mathbf{Q}_{\mathrm{p}} = \mathrm{diag}(\ [\mathbf{10^{10}}]_{1\times 14} \quad [\mathbf{10^{12}}]_{1\times 7}\ ) \tag{52}$$

The covariance is tuned manually, iterative trials with different values are performed whilst controlling the parameters within limits set by engineering judgement; retaining a practical interpretation of the error covariance is desired. $\mathbf{Q}$ is constructed under the expectation that the 19 first modes of the model will have larger excitation than the last 8 modes. The noise level reflects the approximate order of magnitude of the modal states, the standard deviation of the first 19 estimates modes ranges between 1.2 and 60, while for the last 8 it is between 0.05 and 1. The square root of the elements of $\mathbf{R}$ correspond to 5-15% of the standard deviation of $\mathbf{y}(t)$. For $\mathbf{Q}_{\mathrm{p}}$, a higher amount of regularization is prescribed to the seven moments, since they are an order of magnitude higher than the fourteen translational forces.

Fig. 6 shows the estimated acceleration response from the two filters. In the x and y-direction, a very good correspondence is seen. This can be attributed to the physics of the problem: due to the rigidity of the pontoon and the high bending stiffness of the steel truss, the estimates are almost a repetition of signals from the second accelerometer at the same pontoon. The z-direction is more interesting. While the DKF mostly complies with the reference measurement, the accuracy of the JIS estimate is far from satisfactory. Fig. 7 shows that the JIS estimate is inconsistent with the reference in most the higher frequency range. As expected, some discrepancies in the frequency content is also seen for the DKF, but overall it matches well with the reference.

The DKF has the advantage that any numerical instabilities of the force estimate is restrained from inflating due to the control of the force evolution provided by the covariance parameter. On the other hand, the JIS has no prior assumptions on the force evolution, which makes it sensitive to numerical instabilities from ill-conditioning of the system. It is therefore required to carefully select the modes for the reduced order model to reduce the ill-conditioning. It is plausible that the estimation errors of the JIS are caused by ill-conditioning originating from one or more modes. While it is desired to remove any such modes, it may also affect the accuracy of the model representation. We mention that several model configurations were tested, however any overall improvement of the results from the JIS was not observed.

An inspection of the elements of the direct transmission matrix $\mathbf{J}$ indicates a strong local influence, i.e. the response at a pontoon are strongly influenced by the forces on that pontoon. It is possible that when a sensor is removed from the network, the estimated forces deteriorate, in turn affecting the estimated accelerations. The torsional moments (Mx) also have significantly less influence on the output than the forces, though it is also expected that the moments are much larger than the forces.

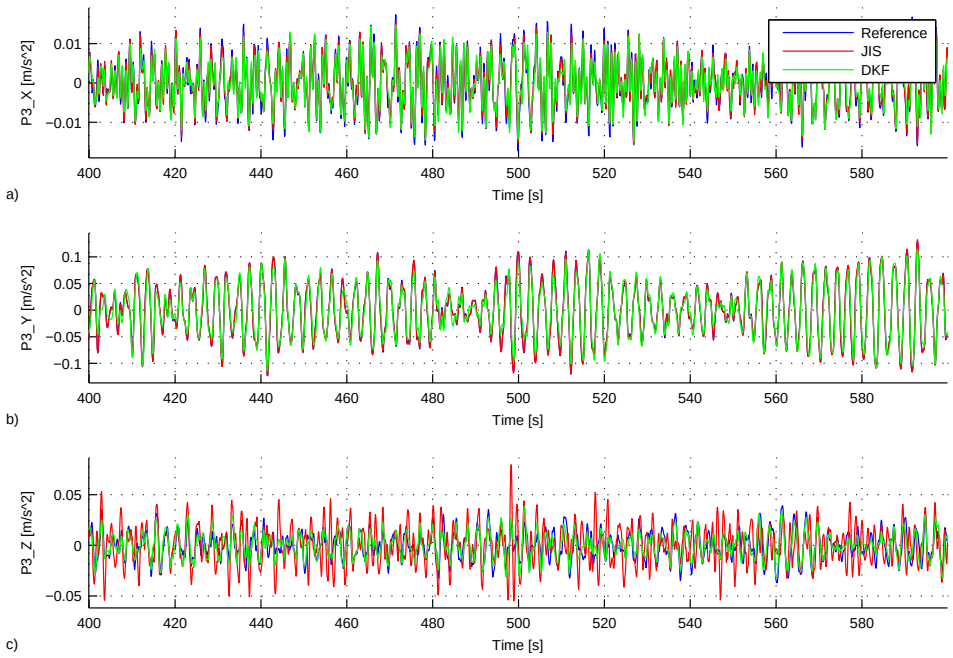

Figure 6: Detail of estimated accelerations in the time domain: a) longitudinal direction; b) transverse direction; c) vertical direction

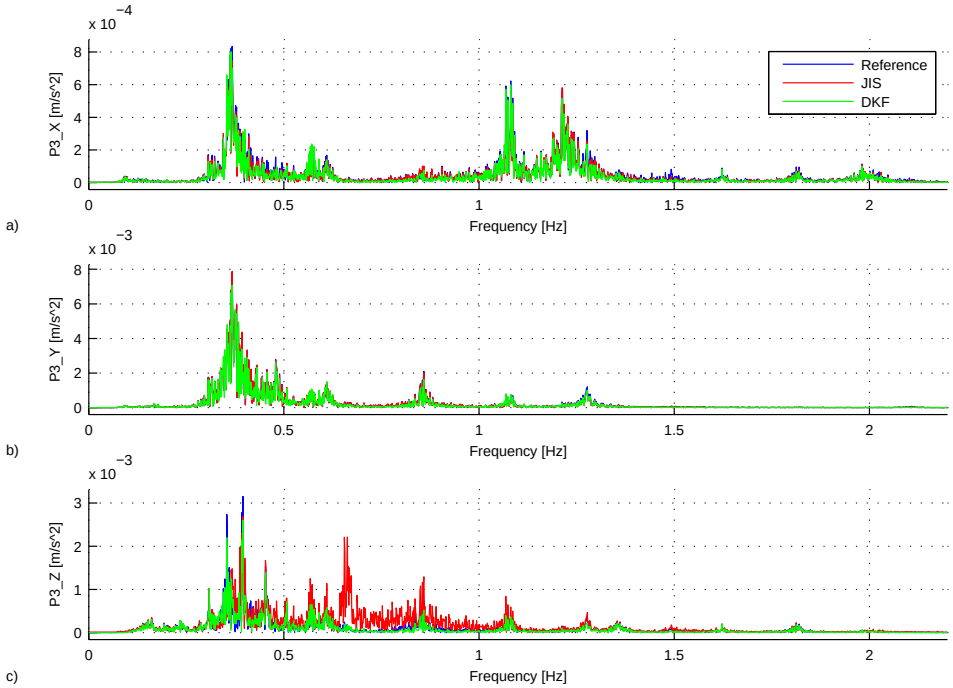

Figure 7: Fourier amplitudes of estimated accelerations: a) longitudinal direction; b) transverse direction; c) vertical direction

The estimated states are briefly examined in an attempt to explain some of the errors in the results. High-pass filtering of the state estimate is done with a 6th order Butterworth filter at 0.12 Hz. Modal displacements for the the five lowermost modes in the model are shown in Fig. 8. Although no reference measurement is available, it is seen both filters agree well, which supports the idea that ill-conditioning of the matrices influencing the force estimates is the reason for the errors.

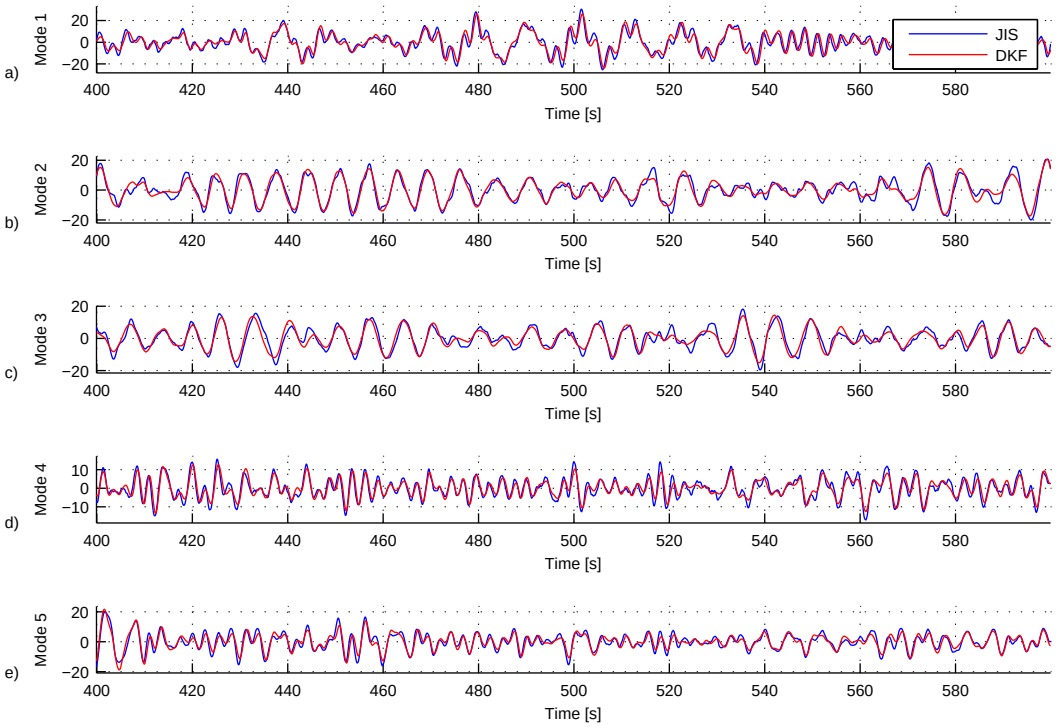

Figure 8: Estimation of the five lowermost modes in the model

An alternative option to using the selected set of hydrodynamic forces is to use an other set of so-called equivalent forces. If the objective is response estimation only, any set of input forces can be used in the identification model as long as they are able to excite all the modes and thereby account for the observed output.

5 Concluding remarks

This paper has shown an application of a joint input-state algorithm and a dual Kalman filter for estimating the response of a floating bridge using acceleration output only. The results show that the acceleration response can be estimated with adequate accuracy with the DKF. With the current sensor network and chosen reduced order model, the acceleration estimate provided by the JIS is prone to instabilities, attributed to ill-conditioning in the matrices used for the system inversion.

Expanding the sensor network could improve the results. More importantly, choosing a suitable set of modes or using another set of equivalent forces is necessary to avoid ill-conditioning.

The authors also aim to extend the studies to input estimation.

References

[1] E. Lourens, C. Papadimitriou, S. Gillijns, E. Reynders, G. De Roeck, and G. Lombaert. Joint input-response estimation for structural systems based on reduced-order models and vibration data from a limited number of sensors. *Mechanical Systems and Signal Processing*, 29:310–327, 2012.

[2] S. Gillijns and B. De Moor. Unbiased minimum-variance input and state estimation for linear discrete-time systems with direct feedthrough. *Automatica*, 43(5):934–937, 2007.

[3] K. Maes, A. Smyth, G. D. Roeck, and G. Lombaert. Uncertainty quantification for joint input-state estimation in structural dynamics. In *5th ECCOMAS Thematic Conference on Computational Methods in Structural Dynamics and Earthquake Engineering (COMPDYN 2015), Crete Island, Greece, 25–27 May*, 2015.

[4] K. Maes, A. Smyth, G. De Roeck, and G. Lombaert. Joint input-state estimation in structural dynamics. *Mechanical Systems and Signal Processing*, 70–71:445–466, 2015.

[5] K. Maes, G. De Roeck, and G. Lombaert. Response estimation in structural dynamics. In *EURODYN 2014: IX INTERNATIONAL CONFERENCE ON STRUCTURAL DYNAMICS*, pages 2399–2406, 2014.

[6] K. Maes, G. De Roeck, A. Iliopoulos, W. Weijtjens, C. Devriendt, and G. Lombaert. Online input and state estimation in structural dynamics. In *Special Topics in Structural Dynamics, Volume 6*, pages 1–10. Springer, 2016.

[7] T. S. Nord, E. Lourens, O. Øiseth, and A. Metrikine. Model-based force identification in experimental ice-structure interaction by means of Kalman filtering. In *EURODYN 2014: Proceedings of the 9th International Conference on Structural Dynamics, Porto, Portugal, 30 June-2 July 2014*. Faculty of Engineering of University of Porto, 2014.

[8] T. S. Nord, E. Lourens, O. Øiseth, and A. Metrikine. Model-based force and state estimation in experimental ice-induced vibrations by means of Kalman filtering. *Cold Regions Science and Technology*, 111:13–26, 2015.

[9] T. S. Nord, O. Øiseth, and E. Lourens. Ice force identification on the nordströmsgrund lighthouse. *Computers & Structures*, 169:24–39, 2016.

[10] K. Maes, A. Iliopoulos, W. Weijtjens, C. Devriendt, and G. Lombaert. Dynamic strain estimation for fatigue assessment of an offshore monopile wind turbine using filtering and modal expansion algorithms. *Mechanical Systems and Signal Processing*, 76-77:592–611, 2016.

[11] P. van der Male and E. Lourens. Operational vibration-based response estimation for offshore wind lattice structures. In *Proceedings of IMAC XXXIII International Modal Analysis Conference*, pages 83–96, 2015.

[12] S. E. Azam, E. Chatzi, and C. Papadimitriou. A dual Kalman filter approach for state estimation via output-only acceleration measurements. *Mechanical Systems and Signal Processing*, 60:866–886, 2015.

[13] S. E. Azam, E. Chatzi, C. Papadimitriou, and A. Smyth. Experimental validation of the dual Kalman filter for online and real-time state and input estimation. In *Model Validation and Uncertainty Quantification, Volume 3*, pages 1–13. Springer, 2015.

[14] S. E. Azam, E. Chatzi, C. Papadimitriou, and A. Smyth. Experimental validation of the kalman-type filters for online and real-time state and input estimation. *Journal of Vibration and Control*, 2015. doi: 1077546315617672.

[15] R. Taghipour, T. Perez, and T. Moan. Hybrid frequency–time domain models for dynamic response analysis of marine structures. *Ocean Engineering*, 35(7):685–705, 2008.

[16] K. A. Kvåle, R. Sigbjörnsson, and O. Øiseth. Modelling the stochastic dynamic behaviour of a pontoon bridge: A case study. *Computers & Structures*, 165:123–135, 2016.

[17] R. E. Kalman. A new approach to linear filtering and prediction problems. *Journal of basic Engineering*, 82(1):35–45, 1960.

[18] K. Maes, E. Lourens, K. Van Nimmen, E. Reynders, G. De Roeck, and G. Lombaert. Design of sensor networks for instantaneous inversion of modally reduced order models in structural dynamics. *Mechanical Systems and Signal Processing*, 52:628–644, 2014.

[19] K. A. Kvåle and O. Øiseth. Structural monitoring of an end-supported pontoon bridge. *(submitted for publication)*, 2016.

[20] Ø. W. Petersen, O. Øiseth, T. S. Nord, and E. Lourens. Model-based estimation of hydrodynamic forces on the Bergsoysund Bridge. In *Proceedings of the 34th IMAC, A Conference and Exposition on Structural Dynamics, Dynamics of Civil Structures, Volume 2*, pages 217–228. Springer, 2016.